Interstitial assessment of aggressive prostate cancer by physio-chemical photoacoustics: An *ex vivo* study with intact human prostates

Shengsong Huang*
Department of Urology, Tongji Hospital, Tongji University School of Medicine, Shanghai 200065, China

Yu Qin*, Yingna Chen, and Jing Pan
Institute of Acoustics, School of Physics Science and Engineering, Tongji University, Shanghai 200092, China

Chengdang Xu and Denglong Wu
Department of Urology, Tongji Hospital, Tongji University School of Medicine, Shanghai 200065, China

Wan-Yu Chao
Faculty of Science, University of Western Ontario, London, ON N6A 3K7, Canada

John T. Wei
Departement of Urology, University of Michigan, Ann Arbor 48109, USA

Scott A. Tomlins
Departement of Pathology, University of Michigan, Ann Arbor 48109, USA

Xueding Wang
Departement of Radiology, University of Michigan, Ann Arbor 48109, USA
Departement of Biomedical Engineering, University of Michigan, Ann Arbor 48109, USA

J. Brian Fowlkes and Paul L. Carson
Departement of Radiology, University of Michigan, Ann Arbor 48109, USA

Qian Cheng[a)]
Institute of Acoustics, School of Physics Science and Engineering, Tongji University, Shanghai 200092, China

Guan Xu[a)]
Department of Urology, Tongji Hospital, Tongji University School of Medicine, Shanghai 200065, China
Departement of Radiology, University of Michigan, Ann Arbor 48109, USA

(Received 28 September 2017; revised 24 April 2018; accepted for publication 10 June 2018; published 23 July 2018)

Purpose: Transrectal ultrasound (TRUS)-guided biopsy is the standard procedure for evaluating the presence and aggressiveness of prostate cancer. TRUS biopsy involves tissue removal, and suffers from low core yield as well as high false negative rate. A less invasive and more accurate diagnostic procedure for prostate cancer is therefore highly desired. Combining the optical sensitivity and ultrasonic resolution to resolve the spatial distribution of the major molecular components in tissue, photoacoustic (PA) technology could be an alternative approach for the diagnosis of prostate cancer. The purpose of this study was to examine the feasibility of identifying aggressive prostate cancer using interstitial PA measurements.

Methods: Seventeen patients with prebiopsy magnetic resonance imaging (MRI), TRUS biopsies, and planned prostatectomies were enrolled in this study. The interstitial PA measurements were achieved using our recently developed needle PA probe, which was inserted into the *ex vivo* prostates in the fashion of a biopsy needle. A total of 70 interstitial PA measurements were acquired. The PA measurements were quantified by a previously established PA physio-chemical analysis (PAPCA) method. The histology has confirmed the nonaggressive and aggressive cancerous conditions at the insertion locations. The diagnostic accuracy was also compared to that provided by the prebiopsy MRI.

Results: The quantitative study shows significant differences between the individual parameters of the nonaggressive and the aggressive cancerous regions ($P < 0.005$). Multivariate analysis of the quantitative features achieved a diagnostic accuracy of 78.6% for differentiating nonaggressive and aggressive prostate cancer tissues.

Conclusions: The proposed procedure has shown promises in the diagnosis of aggressive prostate cancer. © *2018 American Association of Physicists in Medicine* [https://doi.org/10.1002/mp.13061]

Key words: medical imaging, optoacoustics, photoacoustic physio-chemical analysis, photoacoustic spectral analysis, prostate cancer

1. INTRODUCTION

During the past two decades, prostate cancer has become the most commonly diagnosed cancer in American men, with an annual incidence rate much higher than that of any other cancer.[1] Currently, a major challenge to the diagnosis of prostate cancer is to identify aggressive cases in avoidance of metastasis.[2] Transrectal ultrasound (TRUS) guided biopsy is the standard procedure for evaluating the presence and aggressiveness of prostate cancer. During the procedure, 16 or 18 gauge biopsy needles (with diameters of 1.29 and 1.02 mm, respectively) extracts 15 mm biopsy cores from the prostate.[3] Each biopsied tissue is examined by a pathologist and assigned a Gleason score,[4] a highly prognostic architecture-based grading system for prostate cancer. Tissues with Gleason scores equal or larger than 7 (3 + 4) are considered aggressive cancer.[4] Biopsy procedures identifying any aggressive tissues will trigger the therapeutic procedures.[2] Since TRUS imaging can only define the contour of the prostate and the biopsies are typically performed following a predetermined pattern overlaid onto the prostate contour, 20–30% of biopsy procedures were found false negative.[3,5,6] By sampling more than 50 sites, transperineal saturated biopsies have achieved better sensitivity to aggressive prostate cancer.[7] Only 10% of the sample cores are clinically significant, whereas the initial biopsy can still produce 20% false negative diagnoses.[6] Magnetic resonance imaging (MRI) has been introduced to improve the identification of clinically significant prostate cancer in men with initial negative biopsies.[8–10] However, the evaluation of MRI images requires experienced radiologists, and even experienced radiologists have only moderate inter-rater repeatability.[11] The suspicious aggressive cancer regions in MRI still require biopsy core extractions for confirming the disease conditions in the prostates.[12] A diagnostic modality that can assess the aggressiveness of prostate cancer *in vivo* without core extractions could significantly reduce patient anxiety, pain and postprocedure complications.[13]

Photoacoustics (PA) is a technology combining the sensitivity of optical spectroscopy and the resolution of ultrasound imaging. Our recently developed PA spectral analysis (PASA) method[14–17] has demonstrated the capability of determining intraocular tumor types[18] and identifying aggressive prostate cancer.[19] PASA at multiple wavelengths, namely PA physiochemical analysis (PAPCA), has shown the capability of comprehensively analyzing the microarchitectures associated with the major molecular components within the assessed tissue volume. PAPCA has been validated in identifying the diseased conditions during the progression of nonalcoholic fatty liver diseases.[14,15] PASA and PAPCA are potential tools for prostate cancer diagnosis, as the incidence of prostate cancer is associated with both molecular and architectural changes. In our previous study, the PA spectral parameters showed strong correlation with the Gleason scores in human prostate cancer tissues[19] and the vasculature densities in xenograft prostate cancer tumors in mice.[20] Other studies implementing optical modalities including PA imaging have also demonstrated the changes of molecular components such as lipid,[21,22] collagen[23–25] and hemoglobin[21,22,26] in prostate cancer tissue.

However, the strong diffusion of optical energy and attenuation of high-frequency acoustic signals by biological tissue undermined the capability of PA measurements in quantifying the molecular components and microarchitectures in deep prostate tissue. Therefore, the superficial illumination approach used in our previous studies[14,15] is not applicable in the *in vivo* prostate imaging scenario. Most of the previous studies on the PA imaging of prostate cancer were performed with sliced prostate tissues *ex vivo*.[19,21,22] Our recently developed needle PA probe facilitates the delivery of relatively uniform illumination along a fiber optic diffuser, and the reception of the high frequency PA signals with a needle hydrophone from nearby tissues.[27] Such configuration allows the minimally invasive acquisition of PA signals with sufficient temporal length and narrow dynamic range in deep tissue for statistically based PASA.

In this study, for the first time, we have examined the feasibility of interstitial assessment of prostate cancer using the needle PA probe in intact human prostates *ex vivo*. The quantitative analysis methods established in our previous studies[14,15] (i.e., PAPCA) were implemented to the measurements. The quantified diagnostic factors were compared to the pathology results as well as the prebiopsy MRI diagnoses.

2. MATERIALS AND METHODS

2.A. Prebiopsy MRI diagnosis and sample collection

In this study, 17 intact prostate samples were procured in Tongji Hospital in Shanghai, China. All procedures in this study were approved by the Institutional Review Board of the Tongji Hospital. The subjects were provided with written consent. The patients have been examined by multiparametric MRI (Verio 3.0 T, Siemens, Munich, Germany) and TRUS biopsy before the prostatectomy procedures. The configuration of the MRI scanning follows the standards in prostate imaging — reporting and data system.[28] The criteria of the aggressive cancer MRI diagnostic parameters include,[28] (a) the disease anatomies and the enlarged volumes of the prostates revealed by T2-weighted imaging, (b) the presence of hyperintense b-value and hypointense apparent diffusion coefficient in diffusion weighted imaging, and (c) diffusion enhancement in dynamic contrast enhanced imaging. The regions with less yet observable aggressive cancer characteristics were categorized as "suspicious cancerous" regions and also delineated for guiding the biopsy procedures.

The interstitial measurements by needle PA probes were acquired at a total of 70 locations. The measurement locations were marked by a syringe needle after the measurements. The prostates were subsequently diced without interfering with the needles and sliced for histology. The pathology has confirmed that 44 nonaggressive (i.e.,

Gleason < 3 + 4) and 26 aggressive cancerous regions (Gleason score ≥ 3 + 4) were sampled.

2.B. Experiment setup

Figure 1(a) illustrates the experiment setup. In brief, the measurements were acquired by our previously developed needle PA probe[27] consisting of a fiber optic diffuser and a needle hydrophone. The fiber optic diffuser was made from a single optical fiber with a 600 μm core diameter, a 0.39 numerical aperture, and a 2 cm emission end. The needle hydrophone (HNC1500, ONDA Corp., Sunnyvale, CA) has a diameter of 1 mm, and a bandwidth of 1–10 MHz and preamplification of 40 dB. The needle PA probe was inserted into the *ex vivo* prostates at the suspicious nonaggressive and aggressive cancer locations. A tunable optical parametric oscillator (OPO) laser (Phocus Mobile, OPOTEK, Carlsbad, CA) was used to generate illumination in the range of 690–950 and 1200–1700 nm at the intervals of 10 nm. The laser beam with 18 mJ per pulse energy was collimated to approximately 1 mm in diameter and coupled into the fiber optic diffuser. Considering the approximately 30% coupling efficiency, optical energy density of approximately 14 mJ/cm^2 per pulse was delivered to the illumination surface of the needle PA probe surface with an area of approximately 0.377 cm^2 (=π × 600 μm × 2 cm). The signal received by the needle hydrophone was amplified by 40 dB (5072PR, Olympus NDT, Waltham, MA) and averaged 10 times before being recorded by an oscilloscope (TDS 540, Tektronix, Beaverton, OR). With the laser repetition rate of 10 Hz, measurements at each sampling location, including the data transfer between devices took approximately 2 min. A representative signal acquired by the experiment is shown in Fig. 1(b). Similar to the observation in our previous study, the signal possesses narrow dynamic range along the temporal extension corresponding to the length of the fiber optic diffuser.

2.C. Physio-chemical spectra (PCSs) of the nonaggressive and aggressive cancerous locations in the prostate

Our previously developed data processing methods[15] were implemented in this study. The power spectra of the PA signals were calculated using the Welch's approach[29] within the frequency range of 0–8.5 MHz with a step size of 0.1 MHz. The power spectra were arranged in the order of the illumination wavelengths. A 2-dimensional (2D) spectrogram, namely a PCS,[15] was formed for each measurement location. Following the methods in Ref. [15], by comparing to the optical absorption profiles in Fig. 2(c), one can explicitly correlate the stripe patterns in the PCS [marked by the color contours in Figs. 2(a) and 2(b)] with the major molecular components within the assessed tissue volume. The intensities of the stripe patterns, namely PCS fingerprints, presented in pseudo-color, render the relative contents of the components, while the extensions of the fingerprints along the *y*-axis are relevant to the dimensions of the microarchitecture associated with each component.

2.D. Quantification of the diagnostic information in the PCS using PASA

We have successfully quantified the intensities and the extensions of the fingerprints in the PCSs using PASA in our previous study.[15] Figure 3 illustrates the PASA method using the PA signal power spectra at 700 nm. The power spectra were first fit to a linear model. A simple linear model was used as we are only interested in the ratio between the relative high- and low-frequency components. The slope, midband-fit and intercept of the linear models were quantified. The slope represents the heterogeneity formed by the molecular component targeted by the specific wavelength, whereas the intercept and midband-fit represent the relative content of the molecular component. Since two of the three PASA parameters can derive the third, this study only discusses slope and midband-fit. The power spectra in Fig. 3 tend to be overwhelmed by noise above 8.5 MHz and a high pass filter was used to remove the low frequency components generated due to the illumination of the needle hydrophone. The PA frequency range of [0.5, 8.5] MHz was observed.

The PASA slopes and midband-fits were quantified at the center of the PCS fingerprint correlated with each of the major molecular components in the prostates, including hemoglobin (700 nm), lipid (1220 nm), and collagen (1370 nm). The differences between the quantitative features derived from nonaggressive and aggressive cancerous regions were quantified using the one-tailed *t*-tests in MATLAB (Mathworks, Natick, MA). The receiver operating characteristic (ROC) analysis was also performed with the slope values.

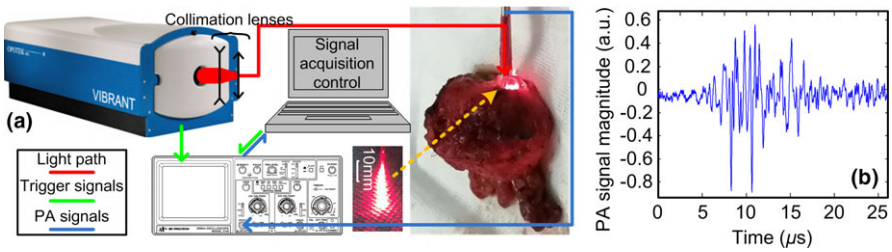

FIG. 1. Experiment system. (a) The laser and the oscilloscope were synchronized. A personal computer was used to store the PA signals. The central bottom insertion shows the illumination by the fiber optic diffuser. (b) Representative signals acquired. [Color figure can be viewed at wileyonlinelibrary.com]

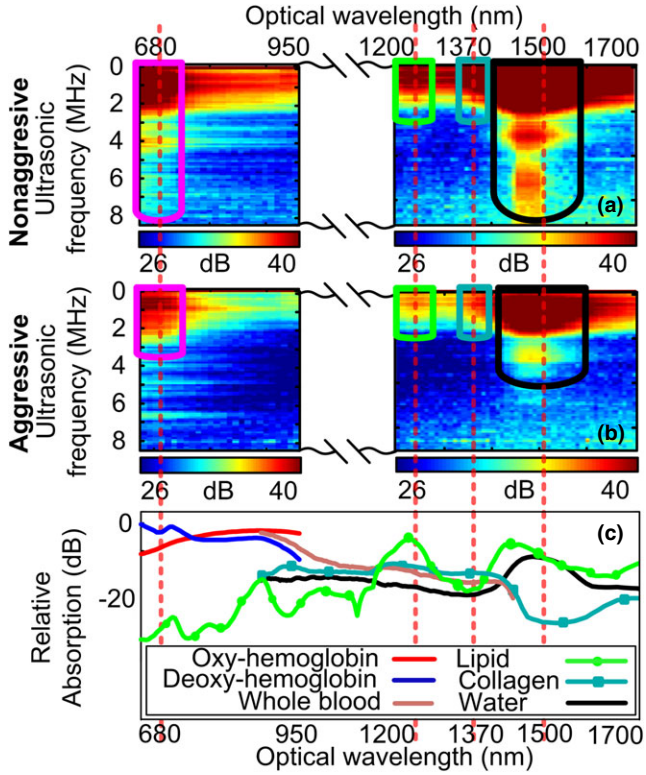

FIG. 2. PCSs acquired by needle PA probes in (a) nonaggressive and (b) aggressive cancerous prostate tissues. (c) The relative optical absorption spectra of the major molecular components in biological tissue.[30] [Color figure can be viewed at wileyonlinelibrary.com]

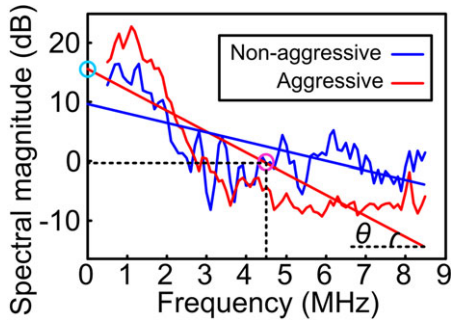

FIG. 3. Illustration of PASA. The PA signals were acquired at 1220 nm. [Color figure can be viewed at wileyonlinelibrary.com]

2.E. Support vector machine (SVM) analysis of the quantitative features

The PASA parameters showing significant difference between the nonaggressive and aggressive prostate tissues were also analyzed in combination using a multivariate analysis method, namely SVM.[31] A MATLAB toolbox, LIBSVM,[32] was implemented to the PASA parameters. This study selected the C-type SVM model. The optimal parameter of the selected SVM, i.e., the regularization parameter C was iteratively searched in the range of 0.1 to 100. Similar to our previous study, the dataset was divided into four groups by the prostate samples (prostates number 1–4, 5–8, 9–12, and 13–17) for blindly testing the proposed categorization based on SVM. The scheme uses three of the four data groups the SVM in turns and the rest one for testing the trained SVM. The accuracy, the sensitivity, and the specificity of the SVM was quantified.

3. RESULTS

3.A. Preliminary diagnosis by MRI and histology results

Figure 4 shows the representative nonaggressive regions, suspicious aggressive cancerous and aggressive cancerous MRI images with the suspicious and aggressive cancerous regions delineated. The MRI diagnosis are listed later in the Table I and compared to the PA diagnosis.

The histology in Fig. 5 shows the decrease of the connective tissues which consist of lipid and collagen [red-pink regions]. The resolvable microscopic features (>150 μm, generating signals within the range of 0–10 MHz) formed by the connective tissues have decreased correspondingly.

3.B. PCSs of nonaggressive and aggressive cancerous prostate tissues

By comparing the PCS fingerprints in Figs. 2(a) and 2(b) to the optical absorption spectra in Fig. 2(c), one is able to correlate hemoglobin, lipid, collagen components with the fingerprints centered at around 700, 1220, and 1370 nm. The fingerprint in the 1400–1500 nm range delineated by the black contours correlated with the overlapping absorption profiles of water and lipid. Since the decoupling of the contribution of the two molecular components in such 2D spectrogram is difficult, the fingerprint at this wavelength range was not quantified.

As shown in Figs. 2(a) and 2(b), the fingerprints in aggressive cancerous PCS, compared to the nonaggressive one, demonstrates lighter color. Such observation indicates that the content of the corresponding molecular components are lower in the aggressive regions. The fingerprints of aggressive cancer tissue also show less extended and the heterogeneous architectures formed by these molecular components have decreased. These observations agree with the histology in Fig. 5.

3.C. Statistics of the quantitative features in PCS

The PASA slopes and midband-fits were quantified from the PCS fingerprints acquired at all the sampled tissue locations. The midband-fits derived at the lipid (1220 nm) and collagen (1370 nm) wavelengths demonstrated slight decrease in aggressive cancerous regions, which agrees with the histology in Fig. 5 and previous studies.[21,23–25] The midband-fits, i.e., the PA signal magnitudes, at 700 nm of the aggressive cancerous tissues demonstrate no significant difference. Such observation agrees with a previous study.[26] The slopes at all the three wavelengths decreased in aggressive cancer regions, which also agree with the histology in Fig. 5.

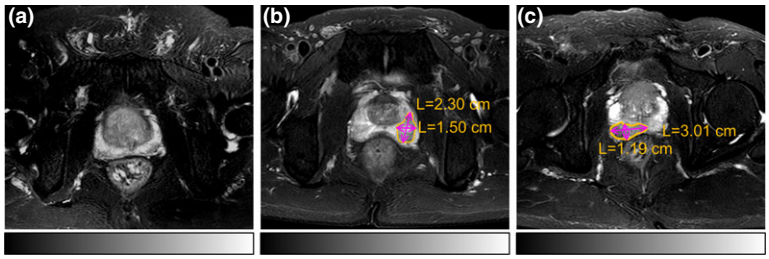

FIG. 4. Representative MRI images with (a) nonaggressive, (b) suspicious aggressive cancerous, and (c) aggressive cancerous regions in prostates. The grayscale is in arbitrary unit. [Color figure can be viewed at wileyonlinelibrary.com]

TABLE I. Comparison between SVM categorization results and the standard pathologic diagnosis. NA: nonaggressive; A: aggressive.

Group #	Prostate #	PA-Meas. #	PA-TP	PA-TN	PA-FP	PA-FN	PA diagnosis	MR diagnosis	Whole prostate pathology
1	1	5	2	2	0	1	A	A	A
	2	5	1	2	1	1	A	A	A
	3	5	1	1	0	3	A	A	A
	4	6	0	6	0	0	NA	A	NA
2	5	4	1	1	1	1	A	A	A
	6	4	0	4	0	0	NA	Suspicious	NA
	7	2	1	1	0	0	A	Suspicious	A
	8	5	0	5	0	0	NA	Suspicious	NA
3	9	3	1	1	0	1	A	Suspicious	A
	10	5	2	1	1	1	A	Suspicious	A
	11	5	1	2	2	0	A	Suspicious	A
	12	4	0	2	2	0	NA	NA	NA
4	13	5	3	2	0	0	A	A	A
	14	3	3	0	0	0	A	A	A
	15	3	0	3	0	0	NA	NA	NA
	16	3	0	3	0	0	NA	Suspicious	NA
	17	3	2	1	0	0	A	Suspicious	A
	Total	70	18	37	7	8			

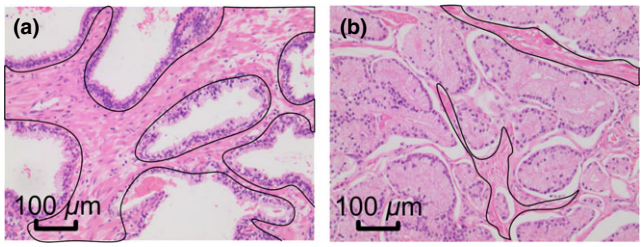

FIG. 5. Representative histology of (a) nonaggressive and (b) aggressive cancerous prostate tissues. The pink regions marked by the black contours were the connective tissues formed by lipid and collagen components. [Color figure can be viewed at wileyonlinelibrary.com]

As mentioned in the method section, the differences between the PASA parameters of nonaggressive regions and aggressive cancerous regions were quantified by one-tailed *t*-tests. Only the slopes at 1220 nm and 1370 nm showed significance. The *P*-values were shown in Figs. 6(e) and 6(f). Such results agree with our previous conclusion[14,15] that PASA slope is a parameter less subject to the uncertain factors such as illumination energy fluctuations.

Figures 7(a), 7(b), 7(c) show The ROC analyses of the slope values derived at each individual wavelengths, respectively. The optimal diagnostic performance is at the point where the ROC curve is farthest from the diagonal line in Fig. 7. Therefore, identifying the aggressive cancerous regions by slopes less or equal than −1.20 at 1220 nm lead to a diagnostic accuracy of 70.0% (49/70) with sensitivity of 88.5% and specificity of 59.1%, respectively. Similarly, identifying the aggressive cancerous regions by slopes at 1370 nm less or equal than −0.952 lead to a diagnostic accuracy of 70.0% (49/70) with sensitivity of 84.6% and specificity of 61.4%, respectively.

3.D. SVM categorization

The regularization parameter in the SVM[32] was determined as 25 by iterative attempts using the fourfold validation scheme. Figure 7(d) shows ROC analysis of the decision values generated by the SVM models. An AUC of 0.811 has been achieved by combining the slopes at all the three wavelengths.

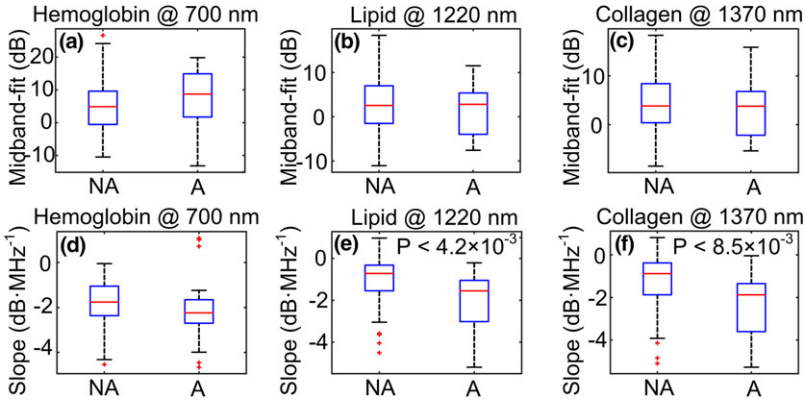

FIG. 6. PASA parameters quantified from the PCSs. The nonaggressive and aggressive cancerous datasets include 44 and 26 samples, respectively.. (a–c) are the boxplots of midband-fits derived from PASA at 700, 1220, and 1370 nm, respectively. (d–f) are the boxplots of slopes derived from PASA at 700, 1220, and 1370 nm, respectively. The red lines represent the medians of the datasets. The upper and lower edges of the boxes are the 25th and 75th percentiles, respectively. The dashed lines extend to the most extreme data points and do not consider outliers. The outliers are plotted as "+". [Color figure can be viewed at wileyonlinelibrary.com]

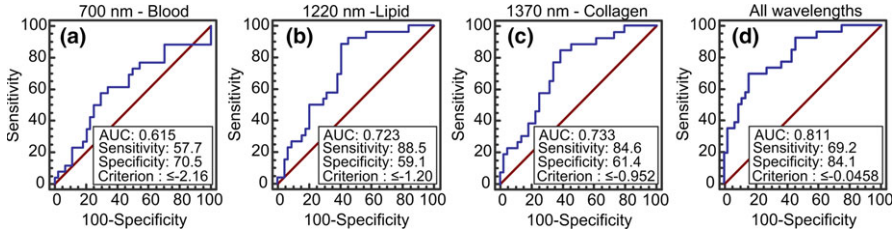

FIG. 7. ROC analysis of the PASA slopes at 1220 nm (a) and 1370 nm (b). [Color figure can be viewed at wileyonlinelibrary.com]

Table I shows the comparison between the pathologic diagnosis, the *in vivo* MRI diagnosis and the *ex vivo* PA diagnosis. The first row shows the grouping of the prostate specimens in the fourfold training-testing cycles. The second and third row shows the serial numbers of the prostate specimens and the number of interstitial PA measurements in each prostate. As shown in Fig. 7(d), using the criteria that the SVM decision values less or equal than −0.0458 indicate aggressive cancers, the diagnostic accuracy for individual interstitial measurements is 78.6% (54/70), with the sensitivity and specificity of 65.4% and 84.1%, respectively. In addition, at least one aggressive cancerous region was correctly identified in the prostates with aggressive cancers. Considering identifying the suspicious regions can effectively guide the TRUS biopsies, MRI has also assisted in identifying most of the aggressive cancer cases, except a false-positive case was found.

4. DISCUSSION

Taking advantage of the optical energy propagation, the interstitial measurements, without tissue removal, could assess tissue volume much larger than that of a biopsy core. The comprehensive assessment of the entire prostate volume thereby becomes possible. One major issue with the interstitial measurement approach is that the needle PA probe has varied penetration at the different wavelengths. And the one dimensional measurement cannot provide sufficient spatial resolution to resolve the assessed volume. However, by assuming that prostate tissue possesses similar optical properties and the cancerous regions are small perturbations to the light propagation, the penetration of a specific wavelength at individual prostates is approximately the same. The comparisons between the PCSs at the same wavelengths are valid.

The prototype needle PA probe will be further miniaturized into the geometry of a biopsy needle. The total detection length of the needle PA probe will be kept as 20 mm, which matches the length of the functional tip of a biopsy needle. Needle hydrophone and fiber optic diffuser with smaller diameters will be integrated into a metal sheath with a side window for light delivery and acoustic signal reception. Such design will be fully compatible with the TRUS guidance for the insertion of the needle PA probes. A smaller detection surface of the hydrophone might reduce the sensitivity of the probe, especially to the high-frequency signal components. The use of thinner optical fiber may also reduce the signal-to-noise ratio of the measurements. Low-noise amplifier will have to be used to ensure the acquisition of sufficient high-frequency signal components encoding the tissue architectures. In addition, we may have to lower the upper limit of the frequency range to minimize the interference of noise floor.

The slopes of the nonaggressive and aggressive cancerous tissues have shown statistically significant differences at both 1220 and 1370 nm. This agrees with the fact that the major change in the cancerous prostate tissues occur

in the tissue microscopic architecture.[4] However, the connective tissues observed in this study are indirect representation the gland architectures, i.e., Gleason grading, which is the standard pathological diagnosis of prostate cancer. Our previous study on PA imaging of prostate cancer tissues with H&E staining of the cellular structures has shown the capability of quantifying the Gleason scores.[33] A previous study[34] has demonstrated that PA imaging can produce images comparable to H&E stained histology by using ultraviolet (UV) wavelengths *in vivo*. UV illumination therefore will allow the direct observation and quantification of the Gleason patterns. The future work of this study is therefore to include PA measurements at UV wavelength for more comprehensive diagnostic information.

The SVM approach combining quantitative parameters at multiple wavelengths has demonstrated better diagnostic performance than differentiating the nonaggressive and aggressive samples using individual wavelengths. This is because the use of multiple parameters improves the separation of the datasets in higher dimension. Therefore, including the measurements at UV wavelength are expected to further improve the accuracy of the proposed diagnostic approach.

5. CONCLUSION AND FUTURE WORKS

This study investigates a minimally invasive and interstitial diagnostic procedure based on a needle PA probe for the identification of aggressive prostate cancer. Experiment results with intact *ex vivo* human prostates have demonstrated the feasibility and decent accuracy of the proposed approaches. Future works will be targeted at miniaturizing the needle PA probe for clinical translation and enriching the diagnostic information by covering more molecular components. The miniaturized needle PA probe will fit perfectly into the established TRUS biopsy procedure and minimize the necessity of tissue core extraction. The proposed interstitial PA measurements approach will reduce the complication of the biopsies, provide reliable diagnosis, and improve the outcomes as well as the quality of life for the patients.

ACKNOWLEDGMENTS

This project is partly supported by National Cancer Institute under grant number: R01CA22282901A1, National Institute of Allergy and Infectious Diseases under grant number: R21AI12209801A1, American Gastroenterological Association Boston Scientific Career Development Technology and Innovation Award, National Institute of Arthritis and Musculoskeletal and Skin Diseases under grant number: 5R01AR060350, National Key Research and Development Program of China under grant number 2017YFC0111400 and National Natural Science Foundation of China under grant numbers 81702962, 11674249, 11574231.

CONFLICTS OF INTEREST

The authors have no conflicts of interest to disclose.

[*]These authors contributed equally to this study.
[a)]Author to whom correspondence should be addressed. Electronic mails: q.cheng@tongji.edu.cn, guanx@umich.edu

REFERENCES

1. Siegel RL, Miller KD, Jemal A. Cancer statistics, 2016. *CA*. 2016;66:7–30.
2. Cooperberg MR, Broering JM, Litwin MS, et al. The contemporary management of prostate cancer in the united states: lessons from the cancer of the prostate strategic urologic research endeavor (capsure), a national disease registry. *J Urol*. 2004;171:1393–1401.
3. Fleshner NE, O'Sullivan M, Fair WR. Prevalence and predictors of a positive repeat transrectal ultrasound guided needle biopsy of the prostate. *J Urol*. 1997;158:505–509.
4. Gleason DF. Histologic grading of prostate cancer: a perspective. *Hum Pathol*. 1992;23:273–279.
5. Rabbani F, Stroumbakis N, Kava BR, Cookson MS, Fair WR. Incidence and clinical significance of false-negative sextant prostate biopsies. *J Urol*. 1998;159:1247–1250.
6. Taira AV, Merrick GS, Galbreath RW, et al. Performance of transperineal template-guided mapping biopsy in detecting prostate cancer in the initial and repeat biopsy setting. *Prostata Cancer Prostatic Dis*. 2010;13:71–77.
7. Merrick GS, Gutman S, Andreini H, et al. Prostate cancer distribution in patients diagnosed by transperineal template-guided saturation biopsy. *Eur Urol*. 2007;52:715–724.
8. Ehdaie B, Shariat SF. Magnetic resonance imaging–targeted prostate biopsy: back to the future. *Eur Urol*. 2013;63:141–142.
9. Fiard G, Hohn N, Descotes J-L, Rambeaud J-J, Troccaz J, Long J-A. Targeted MRI-guided prostate biopsies for the detection of prostate cancer: initial clinical experience with real-time 3-dimensional transrectal ultrasound guidance and magnetic resonance/transrectal ultrasound image fusion. *Urology*. 2013;81:1372–1378.
10. Moore CM, Robertson NL, Arsanious N, et al. Image-guided prostate biopsy using magnetic resonance imaging–derived targets: a systematic review. *Eur Urol*. 2013;63:125–140.
11. Rosenkrantz AB, Ginocchio LA, Cornfeld D, et al. Interobserver reproducibility of the PI-RADS version 2 lexicon: a multicenter study of six experienced prostate radiologists. *Radiology*. 2016;280:793–804.
12. Siddiqui MM, Rais-Bahrami S, Truong H, et al. Magnetic resonance imaging/ultrasound–fusion biopsy significantly upgrades prostate cancer versus systematic 12-core transrectal ultrasound biopsy. *Eur Urol*. 2013;64:713–719.
13. Zisman A, Leibovici DAN, Kleinmann J, Siegel YI, Lindner A. The impact of prostate biopsy on patient well-being: a prospective study of pain, anxiety and erectile dysfunction. *J Urol*. 2001;165:445–454.
14. Xu G, Meng Z-X, Lin JD, et al. The functional pitch of an organ: quantification of tissue texture with photoacoustic spectrum analysis. *Radiology*. 2014;271:130777.
15. Xu G, Meng Z-X, Lin J-D, et al. High resolution physio-chemical tissue analysis: towards non-invasive in vivo biopsy. *Sci Rep*. 2016;6:16937.
16. Xu G, Dar IA, Tao C, Liu X, Deng CX, Wang X. Photoacoustic spectrum analysis for microstructure characterization in biological tissue: a feasibility study. *Appl Phys Lett*. 2012;101:221102–221105.
17. Xu G, Fowlkes JB, Tao C, Liu X, Wang X. Photoacoustic spectrum analysis for microstructure characterization in biological tissue: analytical model. *Ultrasound Med Biol*. 2015;41:1473–1480.
18. Xu G, Xue Y, Özkurt ZG, et al. Photoacoustic imaging features of intraocular tumors: Retinoblastoma and uveal melanoma. *PLoS ONE*. 2017;12:e0170752.
19. Xu G, Davis MC, Siddiqui J, et al. Quantifying Gleason scores with photoacoustic spectral analysis: feasibility study with human tissues. *Biomed Opt Expr*. 2015;6:4781–4789.
20. Kumon RE, Deng CX, Wang X. Frequency-domain analysis of photoacoustic imaging data from prostate adenocarcinoma tumors in a murine model. *Ultrasound Med Biol*. 2011;37:834–839.
21. Dogra VS, Chinni BK, Valluru KS, et al. Multispectral photoacoustic imaging of prostate cancer: preliminary ex-vivo results. *J Clin Imaging Sci*. 2013;3:41.
22. Sinha S, Rao NA, Chinni BK, Dogra VS. Evaluation of frequency domain analysis of a multiwavelength photoacoustic signal for

differentiating malignant from benign and normal prostates. *J Ultrasound Med*. 2016;35:2165–2177.
23. Gleason DF, Mellinger GT. Prediction of prognosis for prostatic adenocarcinoma by combined histological grading and clinical staging. *J Urol*. 2002;167:953–958.
24. Morrison C, Thornhill J, Gaffney E. The connective tissue framework in the normal prostate, B.P.H and prostate cancer: analysis by scanning electron microscopy after cellular digestion. *Urol Res*. 2000;28:304–307.
25. Pu Y, Wang W, Tang G, Alfano RR. Changes of collagen and nicotinamide adenine dinucleotide in human cancerous and normal prostate tissues studied using native fluorescence spectroscopy with selective excitation wavelength. *J Biomed Opt*. 2010;15:047008.
26. Kim SB, Temiyasathit C, Bensalah K, et al. An effective classification procedure for diagnosis of prostate cancer in near infrared spectra. *Exp Syst Appl*. 2010;37:3863–3869.
27. Zhang H, Chao W-Y, Cheng Q, et al. Interstitial photoacoustic spectral analysis: instrumentation and validation. *Biomed Opt Expr*. 2017;8: 1689–1697.
28. Weinreb JC, Barentsz JO, Choyke PL, et al. PI-RADS prostate imaging reporting and data system: 2015, version 2. *Eur Urol*. 2016;69:16–40.
29. Welch P. The use of fast Fourier transform for the estimation of power spectra: a method based on time averaging over short, modified periodograms. *IEEE Trans Audio Electroacoust*. 1967;15:70–73.
30. Wang H-W, Chai N, Wang P, et al. Label-free bond-selective imaging by listening to vibrationally excited molecules. *Phys Rev Lett*. 2011;106:238106.
31. Cortes C, Vapnik V. Support vector machine. *Mach Learn*. 1995;20: 273–297.
32. Chang C-C, Lin C-J. LIBSVM: a library for support vector machines. *ACM Trans Intell Syst Technol*. 2011;2:27.
33. Xu G, Tomlins SA, Siddiqui J, et al. Evaluation of Gleason scores by photoacoustic spectral analysis, 9323: 93231S; 2015.
34. Yao D-K, Maslov K, Shung KK, Zhou Q, Wang LV. In vivo label-free photoacoustic microscopy of cell nuclei by excitation of DNA and RNA. *Opt Lett*. 2010;35:4139–4141.